Two-band Luttinger liquid with spin-orbit coupling: Applications to monatomic chains on surfaces

N. Sedlmayr,* P. Korell, and J. Sirker

Department of Physics and Research Center OPTIMAS, Technical University Kaiserslautern, D-67663 Kaiserslautern, Germany

(Received 1 July 2013; revised manuscript received 25 August 2013; published 7 November 2013)

Recently, monatomic chains on surfaces have been synthesized that show evidence of Luttinger liquid physics. The experimental data point to a dispersion along the chain with four Fermi points. Here we investigate a general low-energy effective Hamiltonian for such a two-band model where SU(2) spin symmetry is broken but time-reversal symmetry persists, as is expected due to the surface geometry. Spin-orbit coupling gives rise to an energy scale $\varepsilon_{\mathrm{SO}}$ much smaller than the Fermi energy ε_F and to spin-nonconserving scattering processes. We derive the generic phase diagram at zero temperature as well as an effective phase diagram at temperatures $\varepsilon_{\mathrm{SO}} < T \ll \varepsilon_F$. For the part of the phase diagram where a Luttinger liquid is found to be stable, the density of states and the spectral function are calculated and discussed in relation to the experimental data.

DOI: 10.1103/PhysRevB.88.195113 PACS number(s): 71.10.Pm, 63.22.Gh, 73.20.At

I. INTRODUCTION

Interacting one-dimensional itinerant electron systems behave very differently from those in higher dimensions. The correct low-energy theory to describe such systems is not Fermi liquid but rather Luttinger liquid theory. In contrast to a Fermi liquid, a Luttinger liquid has collective excitations, shows only a power-law suppression of the occupation number n_k near the Fermi momentum k_F, i.e., a zero quasiparticle weight, and has a separation of spin and charge degrees of freedom.[1,2]

Experimentally, a number of quasi-one-dimensional structures have been investigated with the aim to confirm Luttinger liquid behavior. This has been particularly successful for spin chains, i.e., for systems in which the charge channel is gapped. Prominent examples are various cuprate and organic chains with superexchange coupling constants along the chain direction J being orders of magnitude larger than the interchain couplings $J_\perp$, making them, to a very good approximation, one-dimensional (1D) at temperatures $J_\perp \ll T \ll J$.[3–5] For such systems it has been possible to show that the Luttinger liquid *quantitatively* describes a large number of experimental data ranging from thermodynamic measurements to dynamical response functions.[6–14]

For itinerant electron systems, mounting evidence has also been compiled in recent years verifying the predictions of Luttinger liquid theory, including, in particular, spin charge separation.[15–19] The quasi-one-dimensional systems for which these results have been obtained are, on the one hand, carbon nanotubes, and on the other hand, two-dimensional electron gases confined to a narrow channel by gate electrodes.

Other possible candidates for Luttinger liquids are monatomic chains on surfaces. The best studied examples are gold chains on top of a Si(111) surface.[20–24] While the gold chains were found to exhibit a metal-insulator transition at an energy scale of ~ 100 K so that low-energy Luttinger liquid physics could not be studied,[22,24] a number of important general observations were nevertheless made. In particular, angle-resolved photoemission spectra (ARPES) have shown two closely spaced bands which were first interpreted as a signature of spin-charge separation.[20] Later, however, it was shown by *ab initio* calculations[23] and a more detailed ARPES study[24] that the splitting of the band is caused by spin-orbit coupling.

Very recently, a different surface system has been found which seems to remain metallic down to temperatures of the order of a few Kelvin.[25] Here Au atoms self-organize into chains on a Ge(001) surface, and scanning tunneling spectroscopy (STS) has revealed a density of states (DOS) showing power-law scaling with energy which is indicative of a possible Luttinger liquid state. A subsequent ARPES study showed that the 1D character of the Au chains is indeed exceptionally high. An additional complication in this system arises, however, because the single surface band shows *two* electron pockets,[26,27] a fact which has to be taken into account in a proper theoretical description.

In all these surface systems, Rashba- and Dresselhaus-type spin-orbit couplings are generically expected to be present due to the reduced symmetry.[28,29] In particular, spin-rotational symmetry is expected to be broken and only time-reversal symmetry will persist. Luttinger liquids with spin-orbit interactions have been studied previously in the context of carbon nanotubes[30] and magnetized spin chains and quantum wires.[31,32] There is also a rather extensive literature on one-dimensional models where two bands cross the Fermi surface.[33–46] However, in these works the bands are either assumed to have SU(2) symmetry or to be completely spin split by a magnetic field.

In this paper, we want to consider a generic two-band model with spin-orbit coupling, including all interaction terms which are allowed by time-reversal symmetry. While in the SU(2) symmetric case the phase diagram is to a large extent determined by the renormalization group (RG) flow of marginal interaction terms, most of these interaction terms will become either relevant or irrelevant in the case with only time-reversal symmetry, simplifying the calculation of the phase diagram. On the other hand, four instead of only two independent Luttinger parameters are present once SU(2) symmetry is broken, leading to a much richer phase diagram. Of particular relevance for the experiments on monatomic chains on surfaces is the question of whether a Luttinger liquid phase can survive at all in a surface geometry where the symmetries are reduced. We will show that this is indeed the case, however the phase diagram turns out to be quite rich.

This paper is organized as follows. In Sec. II we introduce a general two-band model with spin-orbit coupling, show how to bosonize it, and look at the interaction terms which are allowed by time-reversal symmetry. In Sec. III we calculate the spin density correlation functions and analyze the simplifications for the specific point in parameter space where the model has an additional SU(2) symmetry. Section IV is devoted to a renormalization group analysis and the subsequent phase diagram of the general model. The spin-flip scattering terms present are found to be slowly oscillating in space so that they can only be ignored at the lowest temperatures. We therefore also present an effective phase diagram at small temperatures where these terms are still present in the RG flow. In Sec. V we look at the spectral function and density of states and try to determine in which part of the phase diagram the system of monatomic chains might be located. Finally, in Sec. VI we conclude.

II. MODEL

A. The noninteracting band structure

We are interested in wires composed of single atoms deposited in surfaces. Such wires have no structural inversion symmetry or inversion center and therefore both Rashba and Dresselhaus-type couplings can be present.[29] For small spin-orbit coupling this will not lead to any drastic effects for the noninteracting band structure. Nonetheless, the breaking of SU(2) symmetry does have important consequences for the interaction terms.[47]

In experiment, the surface band is found to cross the Fermi energy four times, forming two small electron pockets. No microscopic model for the noninteracting band structure, i.e., by downfolding starting from a density functional theory calculation, has been obtained yet. The origin of this band structure is, however, not important for the low-energy effective theory we are going to construct, and we simply take as a given the noninteracting Hamiltonian

$$H_0 = \sum_{\sigma k} (\epsilon_k - \mu) c^\dagger_{\sigma k} c_{\sigma k}, \tag{2.1}$$

where ϵ_k is the dispersion, μ is the chemical potential, and $c^{(\dagger)}_{\sigma k}$ is the fermionic annihilation (creation) operator for particles with spin σ and momentum k. The dispersion before taking spin-orbit interactions into account is supposed to have four spin-degenerate Fermi points $\pm k_{F1}, \pm k_{F2}$ in the Brillouin zone, i.e., $\epsilon_{k_{Fb}} = \mu$ for the "bands" $b = 1,2$. We label the Fermi momenta such that $k_{F1} < k_{F2}$.

We are interested in the regime where the Fermi energy is much larger than the temperature and the energy scale at which the response of the system is tested experimentally. Therefore, we can linearize the dispersion at these Fermi points and introduce two Fermi velocities,

$$v_{Fb} = \left| \frac{d\epsilon}{dk} \right|_{k=k_{Fb}}. \tag{2.2}$$

For clarity, we shall later mostly focus on the situation in which the bands are completely symmetric such that $v_{F1} = v_{F2}$ and where the density-density interactions are also band-independent. The more general case can be treated in a similar way and the necessary generalization is shown in Appendix B.

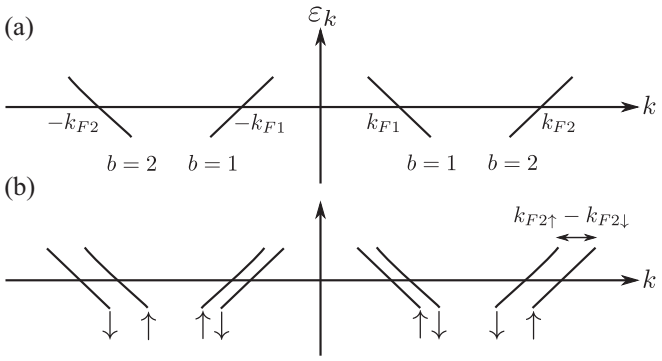

FIG. 1. The dispersion around the Fermi points with the effective band indices 1,2 which are used in the Hamiltonian (2.5). Panel (a) shows the bands without spin-orbit splitting, panel (b) the spin-orbit split bands.

Through the standard linearization procedure in the vicinity of each Fermi point, new fermionic annihilation and creation operators, $c_{\sigma rb}(q)$ and $c^\dagger_{\sigma rb}(q)$, can be defined for particles in band b with spin $\sigma = \pm$ and relative momentum $q = k - r\eta_b k_{Fb}$. Here $r = \pm$ indicates the direction in which the particle is moving, and $\eta_b = (-1)^b$ is an additional band factor depending on whether the slope of the dispersion ϵ_k at the Fermi point $+k_{Fb}$ is positive or negative.

More precisely, we can make the following ansatz using a continuum representation in position space:

$$\psi_\sigma(x) = \sum_{br} e^{ir\eta_b k_{Fb} x} \psi_{\sigma rb}(x), \tag{2.3}$$

where the fields are given by the Fourier transformation

$$\sqrt{a}\psi_{\sigma rb}(x) = \frac{1}{L} \sum_q e^{iqx} c_{\sigma rb}(q), \tag{2.4}$$

with a the lattice spacing.

Following this, the Hamiltonian (2.1) becomes

$$H_0 = \sum_{\sigma rb} r v_{Fb} \int dx\, \psi^\dagger_{\sigma rb}(x)(-i\partial_x)\psi_{\sigma rb}(x), \tag{2.5}$$

a one-dimensional Dirac Hamiltonian with branches labeled by (σrb); see Fig. 1(a).

B. Spin-orbit interactions

To properly treat the spin-orbit interaction, one has to start from a two-dimensional Hamiltonian,

$$H_{2D} = \int dx\, dy\, \boldsymbol{\psi}^\dagger(x,y)[\hat{\epsilon}_x + \hat{\epsilon}_y + V_c(y) + \alpha(\hat{p}_x\sigma_y - \hat{p}_y\sigma_x) + \beta(\hat{p}_x\sigma_x - \hat{p}_y\sigma_y)]\boldsymbol{\psi}(x,y), \tag{2.6}$$

where $\boldsymbol{\psi} = (\psi_\uparrow, \psi_\downarrow)$ and $\hat{\epsilon}_i$ is the kinetic energy operator in the $i = \{x,y\}$ direction, x being longitudinal along the wire. $V_c(y)$ is a confining potential in the transverse direction. The terms in α and β are the Rashba- and Dresselhaus-like spin-orbit coupling terms, respectively. The part $\sim -\hat{p}_y(\alpha\sigma_x + \beta\sigma_y)$ can be treated perturbatively and leads to an effective mixing of higher-lying states into the lowest band. As a consequence,

the velocities of the spin-orbit split bands [see Fig. 1(b)] can become unequal.[30] For a strong confinement $V_c(y)$ this is a small effect which we will neglect in the following. Using this approximation, we are left with a one-dimensional Hamiltonian which can be diagonalized with a spin-orbit induced splitting of the bands given by

$$H_{\rm SO} = \int dx \sum_{r\sigma b} \eta_b r \sigma k_{Fb} \sqrt{\alpha^2+\beta^2}\psi^\dagger_{\sigma br}\psi_{\sigma br}. \quad (2.7)$$

This band splitting gives rise to the definition of an energy scale $\varepsilon^b_{\rm SO} \equiv v_{Fb}k^b_{\rm SO} = \sqrt{\alpha^2+\beta^2}k_{Fb}$ which is much smaller than the Fermi energy ε_F. Here we have assumed that the spin-orbit couplings α, β are the same for both bands.

C. Quartic interaction terms allowed by time-reversal symmetry

A short-range density-density interaction introduces terms which are quadratic in terms of the densities $\rho_{\sigma br} = \psi^\dagger_{\sigma br}\psi_{\sigma br}$ as well as quartic terms in the fermionic operators $\psi_{\sigma br}$ which cannot be written as functions of the densities $\rho_{\sigma br}$. The possible interaction processes depend on the symmetries of the underlying microscopic model. Although the Coulomb interaction itself is SU(2)-symmetric, due to the spin-orbit interactions in Eq. (2.7), scattering between electrons with the same or different spins is no longer equivalent.[47] Furthermore, spin-flip scattering processes become possible. We consider here the most general form of interactions for a system in which only time-reversal symmetry is present. Later, we make two simplifications: (i) We take the velocities of the spin-split bands as being equal, $v_{Fb\sigma} = v_{Fb\bar\sigma}$. As explained above, this is expected to be an excellent approximation for systems in which the confining potential $V_c(y)$ is strong. (ii) We will mainly focus on the case in which the bands are also symmetric, $v_{Fb\sigma} = v_{F\bar b\sigma}$, the generalization to nonsymmetric bands (though still with $k \to -k$ symmetry), however, is straightforward and given in Appendix B.

First we introduce the notation we use to label the different inter- and intraband scattering processes. We retain the usual g_1, g_2, g_4 notation ("g-ology") for the electron directions. Therefore, as usual g_1 refers to processes in which the incoming electrons have different directions and both backscatter. g_2 refers to processes in which the incoming electrons have different directions and there is no backscattering. g_4 refers to incoming electrons of the same direction which do not backscatter. In addition, we use $\bar g$ to mean that the incoming electrons are on different bands and g' to mean that the band index is changed for both electrons. Processes in which one band index changes and the other does not do not contribute (except for one umklapp process treated separately in Appendix D). Finally, we have the spin degrees of freedom. $g_\parallel$ and $g_\perp$ always refer to the spin indices and denote a process in which the electrons have the same spin or different spins, respectively. Where there is no ambiguity and both $g_\parallel$ and $g_\perp$ terms are present, these indices will sometimes be suppressed. g_s is used to refer to a process in which two up spins are scattered to two down spins or vice versa.

1. Density-density-type interactions

Exactly as in the single-band Luttinger liquid, there are g_2 and g_4 density-density interactions, but these no longer need to lie on the same band, thus

$$H_2 = \sum_{\sigma\sigma' br}\int \mathrm{d}x\left[\frac{g_{2b}}{2}\rho_{\sigma' b\bar r}\rho_{\sigma br} + \frac{\bar g_2}{2}\rho_{\sigma'\bar b\bar r}\rho_{\sigma br}\right],$$
$$H_4 = \sum_{\sigma\sigma' br}\int \mathrm{d}x\left[\frac{g_{4b}}{2}\rho_{\sigma' br}\rho_{\sigma br} + \frac{\bar g_4}{2}\rho_{\sigma'\bar b r}\rho_{\sigma br}\right]. \quad (2.8)$$

There are also several backscattering terms which can be rearranged into density-density interactions in the standard way,

$$H_{1\parallel} = -\sum_{\sigma br}\int dx \frac{g_{1\parallel}}{2}\rho_{\sigma b\bar r}\rho_{\sigma br},$$
$$\bar H'_{1\parallel} = -\sum_{\sigma br}\int dx \frac{\bar g'_{1\parallel}}{2}\rho_{\sigma\bar b\bar r}\rho_{\sigma br}, \quad (2.9)$$
$$\bar H'_{4\parallel} = -\sum_{\sigma br}\int dx \frac{\bar g'_{4\parallel}}{2}\rho_{\sigma\bar b r}\rho_{\sigma br},$$

and rescale the $g_{2\parallel}$, $\bar g_{2\parallel}$, and $\bar g_{4\parallel}$ interactions, respectively. These three terms will be assumed to have already been incorporated into their kinematic equivalents, and will not be made explicit in the following. The same will be done for all other equivalent processes we find.

2. Backscattering and interband scattering

With the addition of an extra band, many more backscattering, interband scattering, and umklapp processes become possible, which have no equivalent for a single-band model. As a consequence, we might expect that the extent of a Luttinger liquid phase in the phase diagram—if it survives at all—will be much smaller than that in a single-band model.

We confine ourselves here to the zero-momentum transfer terms, with all other terms suppressed by rapid oscillations in the integrals. Some additional umklapp scattering and backscattering processes which become nonoscillating at special commensurate fillings and thus do contribute at these special fillings are treated in Appendix D. The generic nonoscillating backscattering terms are

$$H_{1\perp} = \sum_{\sigma br}\int dx \frac{g_{1\perp}}{2}\psi^\dagger_{\bar\sigma br}\psi_{\bar\sigma b\bar r}\psi^\dagger_{\sigma b\bar r}\psi_{\sigma br},$$
$$\bar H'_{1\perp} = \sum_{\sigma br}\int dx \frac{\bar g'_{1\perp}}{2}\psi^\dagger_{\bar\sigma br}\psi_{\bar\sigma\bar b\bar r}\psi^\dagger_{\sigma\bar b\bar r}\psi_{\sigma br},$$
$$H'_1 = \sum_{\sigma,\sigma',b,r}\int dx \frac{g'_1}{2}\psi^\dagger_{\sigma'\bar b r}\psi_{\sigma' b\bar r}\psi^\dagger_{\sigma\bar b\bar r}\psi_{\sigma br}, \quad (2.10)$$
$$H'_{2\perp} = \sum_{\sigma,b,r}\int dx \frac{g'_{2\perp}}{2}\psi^\dagger_{\bar\sigma\bar b\bar r}\psi_{\bar\sigma b\bar r}\psi^\dagger_{\sigma\bar b r}\psi_{\sigma br},$$
$$\bar H'_{4\perp} = \sum_{\sigma br}\int dx \frac{\bar g'_{4\perp}}{2}\psi^\dagger_{\bar\sigma br}\psi_{\bar\sigma\bar b r}\psi^\dagger_{\sigma\bar b r}\psi_{\sigma br}.$$

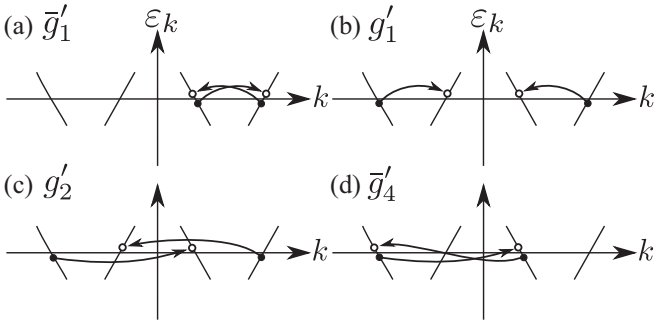

FIG. 2. Additional zero-momentum transfer backscattering and interband scattering processes in a two-band model; see Eq. (2.10). Band structure as for Fig. 1(a).

The additional backscattering and interband processes possible in a two-band, as opposed to a single-band, model are shown schematically in Fig. 2.

3. Single spin-flip scattering

So far, we have just considered the generalization of the usual Coulomb interaction terms to the case of a two-band model. All these terms are symmetric under time reversal,

$$\Psi_{\sigma br} \to \sigma \Psi^\dagger_{\bar{\sigma} b \bar{r}}. \tag{2.11}$$

However, there are also additional spin-flip scattering processes allowed by time-reversal symmetry.

The first cases we want to look at are those in which a single spin is flipped during the scattering process. For every possible $g_\parallel$ and $g_\perp$ scattering process listed in the two preceding sections, such a single spin-flip term can be constructed. For example, a g_1-type single spin-flip process has the form $\sim \psi^\dagger_{\sigma' br}\psi_{\sigma' b\bar{r}}\psi^\dagger_{\bar{\sigma} b\bar{r}}\psi_{\sigma br}$. It is, however, easy to check that this term is always irrelevant. There are a number of similar terms which turn out to be irrelevant as well. The only two single spin-flip terms which, in principle, can become relevant [see Eq. (4.5)] are

$$\begin{aligned} H'_{1sf} &= \frac{G_1}{2}\sum_{\sigma,\sigma',b,r} r\sigma\sigma' \int dx\, \psi^\dagger_{\sigma' \bar{b} r}\psi_{\sigma' b\bar{r}}\psi^\dagger_{\bar{\sigma}\bar{b}\bar{r}}\psi_{\sigma br}, \\ H'_{2sf} &= \frac{G_2}{2}\sum_{\sigma,\sigma',b,r} r\sigma\sigma' \int dx\, \psi^\dagger_{\sigma' \bar{b}\bar{r}}\psi_{\sigma' b\bar{r}}\psi^\dagger_{\bar{\sigma}\bar{b} r}\psi_{\sigma br}. \end{aligned} \tag{2.12}$$

It is important to note that all the single spin-flip terms are slowly oscillating due to the band splitting caused by the spin-orbit coupling; see Fig. 1(b). They can therefore only affect the behavior of the model at intermediate temperatures while we have to drop them anyway at zero temperature. Furthermore, single spin-flip terms are completely forbidden if the velocities of the spin-split bands are equal, $v_{Fb\sigma} = v_{Fb\bar{\sigma}}$. In this case, $\sigma \to \bar{\sigma}$ and $r \to \bar{r}$ are, up to the appropriate shifts in momentum, separate symmetries of the Hamiltonian. As discussed in Sec. II B, the velocities do become unequal once the mixing with other transverse modes is taken into account. We have assumed this to be a small effect and neglect the two scattering terms (2.12) completely in the following.

4. Double spin-flip scattering

The other class of additional scattering terms allowed by time-reversal symmetry, Eq. (2.11), are double spin-flip processes. As for single-flip scattering we can, starting from the usual backscattering, interband scattering, and density-density terms, construct all possible double spin-flip processes. These contributions are

$$\begin{aligned} H_{1s} &= \frac{g_{1s}}{2}\sum_{\sigma br}\int dx\, \psi^\dagger_{\bar{\sigma} br}\psi_{\sigma b\bar{r}}\psi^\dagger_{\bar{\sigma} b\bar{r}}\psi_{\sigma br}, \\ H'_{1s} &= \frac{g'_{1s}}{2}\sum_{\sigma br}\int dx\, \psi^\dagger_{\bar{\sigma}\bar{b} r}\psi_{\sigma b\bar{r}}\psi^\dagger_{\bar{\sigma}\bar{b}\bar{r}}\psi_{\sigma br}, \\ \bar{H}'_{1s} &= \frac{\bar{g}'_{1s}}{2}\sum_{\sigma br}\int dx\, \psi^\dagger_{\bar{\sigma} br}\psi_{\sigma\bar{b}\bar{r}}\psi^\dagger_{\bar{\sigma}\bar{b}\bar{r}}\psi_{\sigma br}. \end{aligned} \tag{2.13}$$

Three g_2 processes also exist. However, they are not kinematically distinct from the g_{1s} interactions. For completeness, they would be g_{2s}, g'_{2s}, and $\bar{g}_{2s}$ and are equivalent to g_{1s}, g'_{1s}, and $\bar{g}'_{1s}$, respectively. In addition, there are two kinematically distinct g_4 processes ($\bar{g}'_{4s}$ is equivalent to $\bar{g}_{4s}$):

$$\begin{aligned} H_{4s} &= \frac{g_{4s}}{2}\sum_{\sigma br}\int dx\, \psi^\dagger_{\bar{\sigma} br}\psi_{\sigma br}\psi^\dagger_{\bar{\sigma} br}\psi_{\sigma br}, \\ \bar{H}_{4s} &= \frac{\bar{g}_{4s}}{2}\sum_{\sigma br}\int dx\, \psi^\dagger_{\bar{\sigma}\bar{b} r}\psi_{\sigma\bar{b} r}\psi^\dagger_{\bar{\sigma} br}\psi_{\sigma br}. \end{aligned} \tag{2.14}$$

The double spin-flip scattering processes are shown schematically in Fig. 3.

Overall, the possible interaction processes consist of the density-density type interactions, the backscattering and interband terms, and the double spin-flip terms. Using bosonization, the density-density terms can be absorbed into the quadratic Luttinger liquid Hamiltonian while the backscattering, interband, and double spin-flip terms will lead to interactions between the bosons. We will see that the spin-orbit induced splitting of the bands, Eq. (2.7), can also be absorbed into the Luttinger liquid Hamiltonian by a shift in the bosonic fields. As a consequence, however, some of the backscattering and all double spin-flip terms will become slowly oscillating in space. The full details are worked out in the next section.

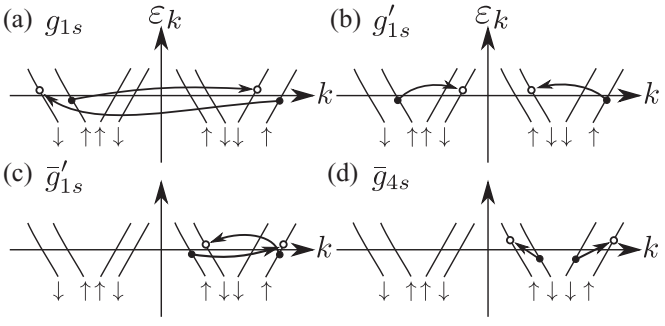

FIG. 3. Double spin-flip processes allowed in a two-band model with time-reversal symmetry; see Eqs. (2.13) and (2.14). Band structure as for Fig. 1(b), with the spin splitting due to spin-orbit coupling made explicit.

D. Bosonization

To bosonize the two-band model, we introduce bosonic fields $\phi_{\sigma rb}(x)$ for each branch,[1,2]

$$\psi_{\sigma rb}(x) = \frac{1}{\sqrt{2\pi\alpha}} e^{ir\sqrt{2\pi}\phi_{\sigma rb}(x)}, \tag{2.15}$$

where the bosonic fields satisfy the following commutation relations:

$$[\phi_{\sigma rb}(x),\phi_{\sigma' r' b'}(x')] = \delta_{\sigma\sigma'}\delta_{rr'}\delta_{bb'}\frac{ir}{2}\,\mathrm{sgn}(x-x'). \tag{2.16}$$

α is a short distance cutoff of the order of the lattice spacing a. For the density operators $\rho_{\sigma rb} = \psi^\dagger_{\sigma rb}\psi_{\sigma rb}$ this leads to the expression $\sqrt{2\pi}\,\rho_{\sigma rb}(x) = -\partial_x\phi_{\sigma rb}(x)$. The Hamiltonian (2.5) of the noninteracting system can now be written in terms of the bosonic fields,

$$H_0 = \sum_{\sigma rb}\frac{v_{Fb}}{2}\int dx[\partial_x\phi_{\sigma rb}(x)]^2. \tag{2.17}$$

Similarly, the spin-orbit term (2.7) can be bosonized, leading to

$$H_{\mathrm{SO}} = -\frac{\sqrt{\alpha^2+\beta^2}}{2\pi}\sum_{\sigma br}\eta_b r\sigma k_{Fb}\int dx\,\partial_x\phi_{\sigma br}. \tag{2.18}$$

We can now also add the density-density-type interactions from Sec. II C1 which are quadratic in the bosonic fields. The Hamiltonian (2.17) including these interaction terms can be written as

$$H_q = \int dz[\partial_x\Phi(x)]^T\mathbf{M}\partial_x\Phi(x), \tag{2.19}$$

where

$$[\Phi]^T = (\phi_{\uparrow 1+},\phi_{\uparrow 1-},\phi_{\downarrow 1+},\phi_{\downarrow 1-},\phi_{\uparrow 2+},\phi_{\uparrow 2-},\phi_{\downarrow 2+},\phi_{\downarrow 2-})$$

and $\mathbf{M}$ is a symmetric 8×8 matrix. The bosonization procedure is thus sufficient to reexpress all but a few contributions in terms of a diagonalizable quadratic bosonic Hamiltonian. The matrix, $\mathbf{M}$, can be written as

$$\mathbf{M} = \frac{1}{2}\begin{pmatrix}\mathbf{M}_1 & \mathbf{M}''\\ \mathbf{M}'' & \mathbf{M}_2\end{pmatrix}, \tag{2.20}$$

where

$$\mathbf{M}_b = \begin{pmatrix} v_{Fb}+\frac{g_{4\parallel b}}{2\pi} & \frac{g_{2\parallel b}}{4\pi} & \frac{g_{4\perp b}}{4\pi} & \frac{g_{2\perp b}}{8\pi}\\ \frac{g_{2\parallel b}}{4\pi} & v_{Fb}+\frac{g_{4\parallel b}}{2\pi} & \frac{g_{2\perp b}}{8\pi} & \frac{g_{4\perp b}}{4\pi}\\ \frac{g_{4\perp b}}{4\pi} & \frac{g_{2\perp b}}{8\pi} & v_{Fb}+\frac{g_{4\parallel b}}{2\pi} & \frac{g_{2\parallel b}}{4\pi}\\ \frac{g_{2\perp b}}{8\pi} & \frac{g_{4\perp b}}{4\pi} & \frac{g_{2\parallel b}}{4\pi} & v_{Fb}+\frac{g_{4\parallel b}}{2\pi}\end{pmatrix}, \tag{2.21}$$

with $b=\{1,2\}$ labeling the bands, and

$$\mathbf{M}'' = \frac{1}{8\pi}\begin{pmatrix} 2\bar{g}_{4\parallel} & 2\bar{g}_{2\parallel} & \bar{g}_{4\perp} & \bar{g}_{2\perp}\\ 2\bar{g}_{2\parallel} & 2\bar{g}_{4\parallel} & \bar{g}_{2\perp} & \bar{g}_{4\perp}\\ \bar{g}_{4\perp} & \bar{g}_{2\perp} & 2\bar{g}_{4\parallel} & 2\bar{g}_{2\parallel}\\ \bar{g}_{2\perp} & \bar{g}_{4\perp} & 2\bar{g}_{2\parallel} & 2\bar{g}_{4\parallel}\end{pmatrix}. \tag{2.22}$$

$\mathbf{M}$ is a real symmetric matrix with real eigenvalues and we can now diagonalize $\mathbf{M}$. The diagonalization can be split up into several steps, and we will show the full procedure to make connections with the standard single-band Luttinger liquid clear.

To begin, we make two unitary transformations. The first is $\phi_{\sigma b\pm}(x) = [\phi_{\sigma b}(x) \mp \theta_{\sigma b}(x)]/\sqrt{2}$. Note that $\theta_{\sigma b}$ is the adjoint of $\phi_{\sigma b}$ and they satisfy $[\phi_{\sigma b}(x),\Pi_{\sigma b}(x')] = i\delta(x-x')$, where $\Pi_{\sigma b}(x) = \partial_x\theta_{\sigma b}(x)$. This first rotation has the effect of uncoupling the two adjoint fields. The second transformation is to rotate to the spin-charge representation: $\phi_{c/s,b}(x) = [\phi_{\uparrow b}(x) \pm \phi_{\downarrow b}(x)]/\sqrt{2}$ [and similarly for the $\theta(x)$ fields]. The effect of these two rotations can be summarized as $\mathbf{M}' = \tilde{\mathcal{U}}^{-1}\mathcal{U}^{-1}\mathbf{M}\mathcal{U}\tilde{\mathcal{U}}$ with $[\Phi'(x)]^T = [\Phi(x)]^T\mathcal{U}\tilde{\mathcal{U}}$. Thus far this just corresponds to the diagonalization procedure for the usual Luttinger liquid[2] applied to the two bands separately.

We now have

$$[\Phi'(x)]^T = (\phi_{s1},\phi_{s2},\theta_{s1},\theta_{s2},\phi_{c1},\phi_{c2}\theta_{c1},\theta_{c2}) \tag{2.23}$$

and the rotated Hamiltonian is defined by the diagonal matrix

$$\mathbf{M}' = \mathrm{diag}\left[\mathbf{M}'_{\phi s},\mathbf{M}'_{\theta s},\mathbf{M}'_{\phi c},\mathbf{M}'_{\theta c}\right]. \tag{2.24}$$

In the following we focus on the symmetric band case in which $\mathbf{M}_1 = \mathbf{M}_2$; see Eq. (2.20). All results are straightforwardly generalizable to the asymmetric case, and the appropriate formulas are given in Appendix B. For the spin and charge ($\nu = \{s,c\}$) sectors, the matrix blocks of $\mathbf{M}'$ are then

$$\mathbf{M}'_{\phi\nu} = \frac{1}{2}\begin{pmatrix}\frac{v_\nu}{K_\nu} & v_{\nu B}\\ v_{\nu B} & \frac{v_\nu}{K_\nu}\end{pmatrix} \tag{2.25}$$

and

$$\mathbf{M}'_{\theta\nu} = \frac{1}{2}\begin{pmatrix}v_\nu K_\nu & v_{\nu A}\\ v_{\nu A} & v_\nu K_\nu\end{pmatrix}. \tag{2.26}$$

Here K_s and K_c are the spin and charge Luttinger parameters for the two bands, and v_s and v_c are the spin and charge velocities. The off-diagonal parameters $\{v_{sA},v_{sB},v_{cA},v_{cB}\}$ describe the coupling between the fields for different bands in the spin and charge sectors and are functions of the various g_2 and g_4 interaction parameters. Their explicit form is given in Eqs. (C1) and (C2) in Appendix C.

In the band symmetric case, we can simply perform another rotation to diagonalize $\mathbf{M}'$ given by $\phi_{\nu 1,2}(x) = [\phi^{\nu+}(x) \mp \phi^{\nu-}(x)]/\sqrt{2}$ and $\theta_{\nu 1,2}(x) = [\theta^{\nu+}(x) \mp \theta^{\nu-}(x)]/\sqrt{2}$. After these additional rotations, the quadratic Hamiltonian becomes diagonal for symmetric bands,

$$H_q = \sum_{\substack{\nu=c,s\\ \beta=\pm}}\frac{u^{\nu\beta}K^{\nu\beta}}{2}\int dx\left[\frac{[\partial_x\phi^{\nu\beta}(x)]^2}{(K^{\nu\beta})^2} + [\Pi^{\nu\beta}(x)]^2\right], \tag{2.27}$$

where $u^{\nu\beta}$ ($K^{\nu\beta}$) are renormalized velocities (Luttinger parameters), the conjugate momenta are given by $\Pi^{\nu\beta}(x) = \partial_x\theta^{\nu\beta}(x)$, and the fields obey bosonic commutation relations

$$[\phi^{\nu\beta}(x),\Pi^{\nu'\beta'}(x')] = i\delta_{\nu\nu'}\delta_{\beta\beta'}\delta(x-x'). \tag{2.28}$$

$\beta = \pm$ label symmetric and antisymmetric combinations of the bands, analogous to charge and spin in the spin subspace.

Finally, we can also rewrite the spin-orbit Hamiltonian (2.18) in terms of the new fields,

$$H_{\rm SO} = -\frac{\sqrt{2(\alpha^2+\beta^2)}}{\pi}\int dx[k_F\partial_x\theta^{s-} + \tilde{k}\partial_x\theta^{s+}] \quad (2.29)$$

with $k_{Fb} = k_F + \eta_b\tilde{k}$. This linear term can simply be removed by the following shift:

$$\theta^{s-} \to \theta^{s-} + \frac{\sqrt{2}k_F x}{u^{s-}K^{s-}}\frac{\sqrt{\alpha^2+\beta^2}}{\pi} \quad (2.30)$$

and similarly for θ^{s+} so that $H_q + H_{\rm SO} \to H_q + \text{const}$. However, this shift has to be carefully taken into account for the nonquadratic interaction terms. As we will see below, it will induce slow oscillations in space for some of these terms.

E. Bosonized interactions

In addition to the quadratic bosonic Hamiltonian, we have the set of backscattering, interband scattering, and double spin-flip scattering interactions, Eqs. (2.10)–(2.14). The vertex operator, Eq. (2.15), allows a straightforward bosonization of these interactions. First, the g_1 backscattering interactions become

$$\begin{aligned}
H_{1\perp} &= \frac{g_{1\perp}}{(\pi\alpha)^2}\int dx\cos[\sqrt{4\pi}\phi^{s+}]\cos[\sqrt{4\pi}\phi^{s-}],\\
H'_{1\parallel} &= -\frac{g'_{1\parallel}}{(\pi\alpha)^2}\int dx\cos[\sqrt{4\pi}\theta^{s-}]\cos[\sqrt{4\pi}\theta^{c-}],\\
H'_{1\perp} &= \frac{g'_{1\perp}}{(\pi\alpha)^2}\int dx\cos[\sqrt{4\pi}\phi^{s+}]\cos[\sqrt{4\pi}\theta^{c-}],\\
\bar{H}'_{1\perp} &= \frac{\bar{g}'_{1\perp}}{(\pi\alpha)^2}\int dx\cos[\sqrt{4\pi}\phi^{s+}]\cos[\sqrt{4\pi}\theta^{s-}].
\end{aligned} \quad (2.31)$$

Secondly, there is a g_2 process,

$$H'_{2\perp} = \frac{g'_{2\perp}}{(\pi\alpha)^2}\int dx\cos[\sqrt{4\pi}\phi^{s-}]\cos[\sqrt{4\pi}\theta^{c-}]. \quad (2.32)$$

Lastly, there is a g_4 process,

$$\bar{H}'_{4\perp} = \frac{\bar{g}'_{4\perp}}{(\pi\alpha)^2}\int dx\cos[\sqrt{4\pi}\phi^{s-}]\cos[\sqrt{4\pi}\theta^{s-}]. \quad (2.33)$$

Several of these terms are shown schematically in Fig. 2.

The allowed double spin-flip backscattering interactions, Eq. (2.13), in bosonized form are given by

$$\begin{aligned}
H_{1s} &= \frac{g_{1s}}{(\pi\alpha)^2}\int dx\cos[\sqrt{4\pi}\theta^{s+}]\cos[\sqrt{4\pi}\theta^{s-}],\\
H'_{1s} &= \frac{g'_{1s}}{(\pi\alpha)^2}\int dx\cos[\sqrt{4\pi}\theta^{s+}]\cos[\sqrt{4\pi}\theta^{c-}],\\
\bar{H}'_{1s} &= \frac{\bar{g}'_{1s}}{(\pi\alpha)^2}\int dx\cos[\sqrt{4\pi}\phi^{s-}]\cos[\sqrt{4\pi}\theta^{s+}].
\end{aligned} \quad (2.34)$$

The last two spin-flip interactions which contribute, Eq. (2.14), are

$$\bar{H}_{4s} = \frac{\bar{g}_{4s}}{(\pi\alpha)^2}\int dx\cos[\sqrt{4\pi}\phi^{s+}]\cos[\sqrt{4\pi}\theta^{s+}] \quad (2.35)$$

and

$$H_{4s} = \frac{g_{4s}}{(\pi\alpha)^2}\int dx\left\{\prod_\beta \cos[\sqrt{4\pi}\theta^{s\beta}]\cos[\sqrt{4\pi}\phi^{s\beta}] + \prod_\beta \sin[\sqrt{4\pi}\theta^{c\beta}]\sin[\sqrt{4\pi}\phi^{c\beta}]\right\}. \quad (2.36)$$

If we now shift the θ^{s-} and θ^{s+} fields to compensate for the spin splitting in the bands [see Eq. (2.30)], then the backscattering terms $H'_{1\parallel}$, $\bar{H}'_{1\perp}$, and $\bar{H}'_{4\perp}$ and all the double spin-flip processes become slowly oscillating. These oscillations will suppress the interactions at the lowest temperatures, when the correlation length $\xi \sim v_F/T \gg 1/k^b_{\rm SO}$. They will, however, still be present in the RG flow at intermediate temperatures, $\varepsilon^b_{\rm SO} \ll T \ll \varepsilon_F$. In Sec. IV, we will consider the phase diagram at zero temperature as well as an effective phase diagram in the intermediate temperature regime.

III. SU(2) SYMMETRY AND SPIN DENSITY CORRELATION FUNCTIONS

Before we continue with the calculation of the phase diagram in the presence of the interaction terms, we want to study first the spin-spin correlation functions for the quadratic Hamiltonian (2.27). In particular, we want to find out what conditions are imposed on the parameters of the two-band model at the point where SU(2) spin symmetry is restored. Contrary to the usual single-band model where this leads to $K_s = 1$, it is not *a priori* clear if a similar condition also holds in the two-band case.

For the following calculations it is convenient to express the new fields $\phi^{\nu\beta}$ and $\theta^{\nu\beta}$, introduced to diagonalize the quadratic part of the Hamiltonian, in terms of new chiral fields determined by

$$\phi^{\nu\beta}_\delta = \frac{1}{\sqrt{2}}\left(\frac{\phi^{\nu\beta}}{\sqrt{K^{\nu\beta}}} - \delta\sqrt{K^{\nu\beta}}\theta^{\nu\beta}\right), \quad (3.1)$$

where $\delta = \pm$ is once again a direction index. These new fields describe the chiral excitations of the system moving either to the left, $\delta = -$, or to the right, $\delta = +$. In this basis, the appropriate time-ordered correlation functions of the bosonic fields are given by

$$\begin{aligned}
G_{\nu\beta\delta}(x,t) &\equiv \left\langle T_t\left[\phi^{\nu\beta}_\delta(x,t) - \phi^{\nu\beta}_\delta(0)\right]^2\right\rangle\\
&= \frac{1}{\pi}\ln\left[\frac{\alpha + \text{sgn}(t)i(u^{\nu\beta}t - \delta x)}{\alpha}\right].
\end{aligned} \quad (3.2)$$

Using this correlation function, one can calculate the correlations of the oscillating parts of the spin density waves,

$$S^j_{\rm SDW}(x,t) = \sum_{\substack{\sigma,\sigma';\\(r,b)\neq(r',b')}} e^{i(r'\eta_{b'}k_{Fb'} - r\eta_b k_{Fb})x}\psi^\dagger_{\sigma rb}(x,t)\sigma^j_{\sigma\sigma'}\psi_{\sigma' r' b'}(x,t), \quad (3.3)$$

where σ^j are the Pauli matrices for $j = x,y,z$.

TABLE I. The exponents for different scattering processes in the spin density wave correlations; see Eq. (3.4).

Charge exponent	Spin exponent
$\varepsilon_c = \frac{1}{2}\left(K^{c+} + K^{c-}\right)$	$\varepsilon_s^z = \frac{1}{2}\left(K^{s+} + K^{s-}\right)$
	$\varepsilon_s^x = \frac{1}{2}\left(\frac{1}{K^{s+}} + \frac{1}{K^{s-}}\right)$
$\bar{\varepsilon}_c = \frac{1}{2}\left(K^{c+} + \frac{1}{K^{c-}}\right)$	$\bar{\varepsilon}_s^z = \frac{1}{2}\left(K^{s+} + \frac{1}{K^{s-}}\right)$
	$\bar{\varepsilon}_s^x = \frac{1}{2}\left(K^{s-} + \frac{1}{K^{s+}}\right)$
$\varepsilon_{cf} = \frac{1}{2}\left(K^{c-} + \frac{1}{K^{c-}}\right)$	$\varepsilon_{sf}^z = \frac{1}{2}\left(K^{s-} + \frac{1}{K^{s-}}\right)$
	$\varepsilon_{sf}^x = \frac{1}{2}\left(K^{s+} + \frac{1}{K^{s+}}\right)$

For the oscillating parts of the spin density wave correlation function in the x or z direction (in the y direction it is trivially equivalent to that in x), we obtain

$$\begin{aligned}\left\langle S_{\mathrm{SDW}}^{x,z}(x,0) S_{\mathrm{SDW}}^{x,z}(0,0)\right\rangle &= \frac{1}{(\pi\alpha)^2}\left[\sum_b \frac{\cos[2k_{Fb}x]}{|x/\alpha|^{\varepsilon_c+\varepsilon_s^{x,z}}} + \frac{\cos[(k_{F1}+k_{F2})x]}{|x/\alpha|^{\bar{\varepsilon}_c+\bar{\varepsilon}_s^{x,z}}}\right.\\ &\left. + \frac{\cos[(k_{F1}-k_{F2})x]}{|x/\alpha|^{\varepsilon_{cf}+\varepsilon_{sf}^{x,z}}}\right]. \end{aligned} \tag{3.4}$$

There are three different types of competing density waves present. The first is backscattering which preserves the band index, with exponents $\varepsilon_\nu^{x,z}$, the direct analog of backscattering in a single-band system. The second is backscattering which mixes the bands, $\bar{\varepsilon}_\nu^{x,z}$. Finally, there is a forward scattering process which scatters between the bands, $\varepsilon_{\nu f}^{x,z}$. The exponents are summarized in Table I.

For SU(2) symmetry to hold, the spin-density–spin-density correlation should be the same with respect to any spatial direction. This is clearly always fulfilled for the charge exponents, but it gives us a set of conditions for the spin exponents. In the case of equivalent bands (the more general case is explained in Appendix B), this imposes

$$K^{s+} = K^{s-} = 1, \tag{3.5}$$

which is indeed in direct analogy to the usual single-band Luttinger liquid condition.

IV. PHASE DIAGRAM

To see how the backscattering terms, Eq. (2.10), and the double spin-flip terms, Eqs. (2.13) and (2.14), change the behavior of the system, we perform a first-order RG analysis on them. Note that away from the SU(2)-symmetric point, the terms become unambiguously irrelevant or relevant, forgoing the need for a more complicated second-order treatment.

The standard first-order renormalization group analysis yields for the interactions of the system a set of independent equations for the flow of the coupling constants g_i, $\bar{g}_i$, and $\bar{g}_i'$ under a change of the length scale l,

$$\frac{1}{g_i}\frac{dg_i}{dl} = 2 - \gamma_i\,. \tag{4.1}$$

The $\{\gamma_i\}$ are then the scaling dimensions of the corresponding scattering terms. These scaling dimensions can be easily extracted by power counting. Several of the interaction terms are always irrelevant, or at best marginal in an SU(2) symmetric system, and we first list these together here:

$$\begin{aligned}\bar{\gamma}_{4\perp}' &= K^{s-} + \frac{1}{K^{s-}}, \quad \bar{\gamma}_{4s} = K^{s+} + \frac{1}{K^{s+}},\\ \gamma_{4s} &= K^{s+} + \frac{1}{K^{s+}} + K^{s-} + \frac{1}{K^{s-}}.\end{aligned} \tag{4.2}$$

The remaining backscattering scaling dimensions are

$$\begin{aligned}\gamma_{1\perp} &= K^{s+} + K^{s-},\\ \gamma_{1\parallel}' &= \frac{1}{K^{s-}} + \frac{1}{K^{c-}}, \quad \gamma_{1\perp}' = K^{s+} + \frac{1}{K^{c-}},\\ \bar{\gamma}_{1\perp}' &= K^{s+} + \frac{1}{K^{s-}}, \quad \gamma_{2\perp}' = K^{s-} + \frac{1}{K^{c-}}.\end{aligned} \tag{4.3}$$

Similarly, we find for the double spin-flip scattering terms

$$\begin{aligned}\gamma_{1s} &= \frac{1}{K^{s+}} + \frac{1}{K^{s-}}, \quad \gamma_{1s}' = \frac{1}{K^{s+}} + \frac{1}{K^{c-}},\\ \bar{\gamma}_{1s}' &= K^{s-} + \frac{1}{K^{s+}}.\end{aligned} \tag{4.4}$$

Finally, the two possibly relevant single spin-flip interactions which could modify the intermediate phase diagram, see Eq. (2.12), have scaling dimensions

$$\begin{aligned}\gamma_{1sf}' &= \frac{1}{K^{c-}} + \frac{1}{4}\left(K^{s+} + \frac{1}{K^{s+}} + K^{s-} + \frac{1}{K^{s-}}\right),\\ \gamma_{2sf}' &= K^{c-} + \frac{1}{4}\left(K^{s+} + \frac{1}{K^{s+}} + K^{s-} + \frac{1}{K^{s-}}\right).\end{aligned} \tag{4.5}$$

All other single spin-flip processes have a scaling dimension $\gamma_{sf} > 2$ and are thus irrelevant.

For a relevant interaction term, the coupling constant grows while lowering the temperature. Thus the bosonic fields present in this interaction will get pinned to the values which minimize the energy, leading to a gap in the corresponding dual mode. We will follow the standard notation where CxSy is a phase of the system with x gapless charge and y gapless spin modes.[38] Note, however, that of course only one of the dual fields, $\phi^{\nu\beta}$ and $\theta^{\nu\beta}$, can be pinned since the commutation relation between them must be preserved.[48]

As we are interested in models without SU(2) symmetry, it is most convenient to plot the phase diagram for $K^{s\pm}$ with K^{c-} a parameter. To establish the phase diagram, we define for convenience

$$\chi = \frac{K^{c-}}{2K^{c-} - 1}. \tag{4.6}$$

The large number of scattering terms for the two-band model leads to a very rich phase diagram, which contains a Luttinger liquid region; see Fig. 4. This region becomes enlarged for strong interactions as the horizontal and vertical separatrixes are K^{c-}-dependent and for $K^{c-} \to 0.5$, $\chi \to \infty$. That is, these separatrixes are completely removed from the phase diagram for $K^{c-} \leqslant 0.5$. Conversely, as $K^{c-} \to 1$ we have $\chi \to 1$, reducing the extent of the C2S2 phase.

However, this phase diagram will only hold at the lowest temperatures where the slowly oscillating scattering terms containing the θ^{s-} and θ^{s+} fields can be neglected. At temperatures $\varepsilon_{\mathrm{SO}}^b \ll T \ll \varepsilon_F$ these scattering terms also have to be kept,[49] leading to additional sections of the phase diagram where some modes will appear thermally activated and the

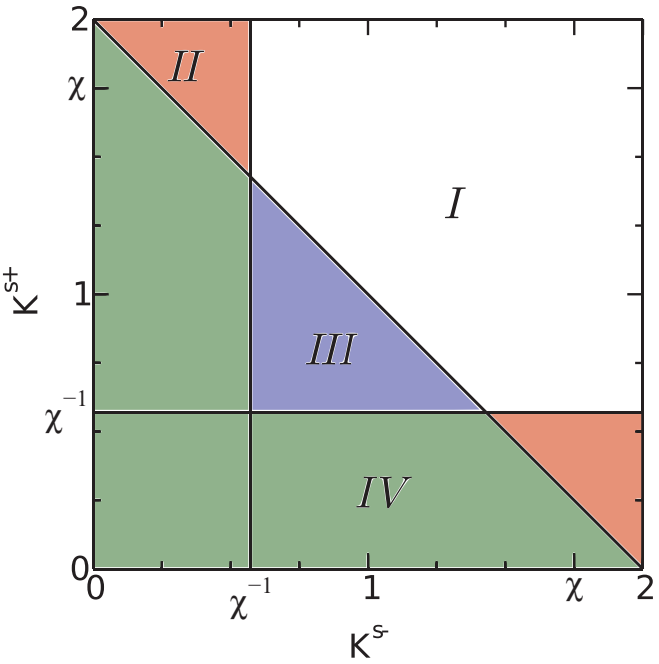

FIG. 4. (Color online) The phase diagram at temperatures $T \ll \varepsilon_{\mathrm{SO}}$ with χ as defined in (4.6). Here we have used $K^{c-} = 0.7$. The solid lines are the separatrixes between different phases and the C2S2 Luttinger liquid phase is the unshaded white region. The red regions marked (II) are C1S1 phases, blue (III) are C2S0 phases, and green (IV) are C1S0 phases.

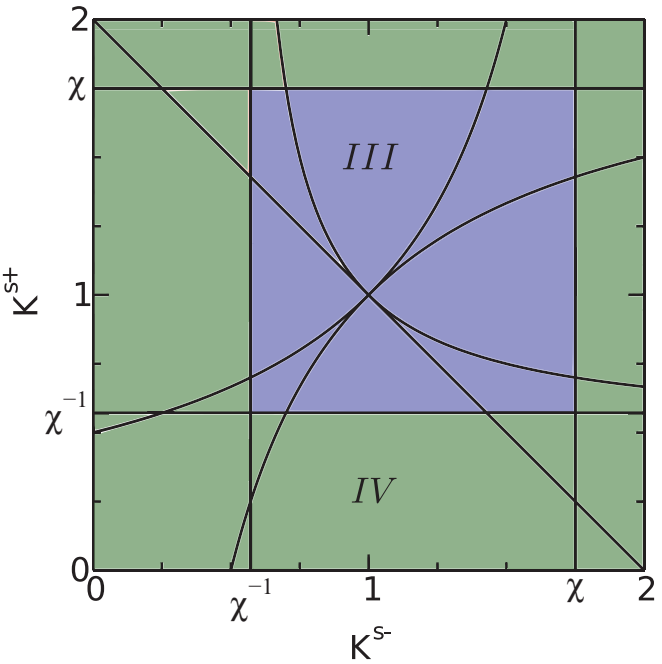

FIG. 5. (Color online) The effective phase diagram at $\varepsilon^b_{\mathrm{SO}} \ll T \ll \varepsilon_F$. At these temperatures the slowly oscillating interaction terms have to be kept and lead to additional phases where modes appear to be thermally activated. As in Fig. 4 we exemplarily show the diagram for $K^{c-} = 0.7$. The solid lines are the separatrices between different phases. The blue regions marked (III) are C2S0 phases, and green (IV) are C1S0 phases.

corresponding spectral weight strongly suppressed. A well known example for such behavior is the one-band Hubbard model solvable by the Bethe ansatz. At filling $n = 1$ and on-site interaction $U > 0$ the charge mode is gapped (Mott insulator) while there is no gap away from half-filling. However, at $n = 1 \pm \epsilon$ with $|\epsilon| \ll 1$ the cosine scattering term responsible for the Mott transition will oscillate only very slowly. As a consequence, the charge compressibility will look thermally activated as in the half-filled case at high and intermediate temperatures with a steep increase visible only at the lowest temperatures.[50] The effective phase diagram, including the phases which appear to be gapped at temperatures $\varepsilon^b_{\mathrm{SO}} \ll T \ll \varepsilon_F$, is shown in Fig. 5.

In the experiments considering self-organized gold chains on a Ge(001) surface, a Luttinger liquid (C2S2) phase appears to be seen.[25] This is surprising given the large number of scattering terms for a system with four Fermi points, although our results clearly show that it is not impossible if the Luttinger liquid parameters are in the right range. However, these restrictions on the Luttinger parameters also mean that the structure of the spin density waves in the Luttinger liquid are constrained. In particular, we are interested in what these constraints mean for the decay of the in-plane and perpendicular components of the spin correlation function. Physically, we might expect that the spins are lying mainly within the surface with the perpendicular component being comparatively smaller. This can be used as a consistency check to see if the formation of a Luttinger liquid in this surface system is reasonable.

If we assume that the system is in the low-temperature C2S2 phase, shown in Fig. 4, then we have a set of constraints on the Luttinger parameters. The separatrixes of this phase are composed of the $\gamma'_{1\perp}$, $\gamma'_{2\perp}$, and $\gamma_{1\perp}$ interaction processes. There are two constraints which involve the charge Luttinger parameter:

$$K^{s+} > \chi^{-1} \text{ and } K^{s-} > \chi^{-1}. \tag{4.7}$$

Additionally we require the following to hold between the spin Luttinger parameters:

$$K^{s+} + K^{s-} > 2. \tag{4.8}$$

From these general considerations some conclusions follow about the spin density wave correlation functions in the Luttinger liquid phase; see Eq. (3.4). If $K^{s+}K^{s-} > 1$—which is true for most of the C2S2 phase—then we find for the intra band exponents $1 \leqslant \varepsilon^z_s > \varepsilon^x_s$. That is, the spin-density–spin-density correlation function decays quicker in the out-of-plane direction, as one may expect. For interband backscattering, $\bar{\varepsilon}^{x,z}_s$, neither in plane nor out of plane correlations are necessarily preferred. For forward scattering both $\varepsilon^{x,z}_{sf} \geqslant 1$, but the relation between them is not fixed. In general, we can say nothing for the relative in- and out-of-plane power laws of the interband forward scattering terms. The actual spin order in the system will be the result of the competition between these possible processes.

TABLE II. Pair operators and density waves which lead to algebraically decaying correlations in phases with two gapped modes. All possible pairs of gapped modes for the zero-temperature phase diagram are included.

Phase	Pinned fields	Pair operator	Density waves
C2S0	ϕ^{s-}, ϕ^{s+}	$O_{S,\sigma;rb,rb}$, $O_{S,\sigma;rb,\bar{r}b}$	$O_{\mathrm{CDW},\sigma;rb,\bar{r}b}$
C2S0	ϕ^{s-}, θ^{s+}	$O_{S,\sigma;rb,rb}$	$O_{\mathrm{SDW},\sigma;rb,\bar{r}\bar{b}}$
C1S1	θ^{c-}, ϕ^{s-}	$O_{T,\sigma;rb,r\bar{b}}$	$O_{\mathrm{SDW},\sigma;rb,\bar{r}\bar{b}}$
C1S1	θ^{c-}, θ^{s+}	$O_{S,\sigma;rb,r\bar{b}}$, $O_{T,\sigma;rb,\bar{r}b}$	$O_{\mathrm{SDW},\sigma;rb,\bar{r}\bar{b}}$

A. Characterization of phases with gapped modes

If the system is in a phase where at least one mode is gapped, single-particle correlations will in general no longer be described by power laws but will decay exponentially.[48] In particular, the spectral function will always show exponential decay in phases with gapped modes. However, if we consider many-particle correlations which do not involve the gapped modes, then they will still behave as power laws. It is therefore standard practice to characterize a gapped phase by the many-particle correlation function which shows the slowest decay.

To consider a concrete example, let us assume that the $g_{1\perp}$ backscattering term, Eq. (2.31), is relevant. Then the fields ϕ^{s+} and ϕ^{s-} are pinned to the values which minimize the energy of this backscattering term. Every correlation function which involves at least one of the dual fields θ^{s+} or θ^{s-} is then exponentially decaying. The many-body correlation functions $\langle O(x,t)O(0,0)\rangle$ which will still show a power-law decay are those with an operator O which does not contain these two dual fields. All operators for which this is true can be determined by using the bosonization dictionary given in Appendix A. For the considered example we find that the two singlet pair operators $O_{S,\sigma;br,br} = \Psi_{\sigma br}\Psi_{\bar{\sigma} br}$ and $O_{S,\sigma;br,b\bar{r}} = \Psi_{\sigma br}\Psi_{\bar{\sigma} b\bar{r}}$ as well as the charge density wave $O_{\mathrm{CDW},\sigma;br,b\bar{r}} = \Psi^{\dagger}_{\sigma br}\Psi_{\sigma b\bar{r}}$ will be the pair correlation functions which decay with a power law. Which one of these shows the slowest decay depends on the values of the Luttinger parameters.

For all other phases with two gapped modes, we can use a similar procedure. In addition to the already introduced singlet pair operator O_S and charge density wave operator O_{CDW}, also the triplet pair correlations with $O_{T,\sigma;rb,r'b'} = \psi_{\sigma rb}\psi_{\sigma r'b'}$ and the spin density wave $O_{\mathrm{SDW},\sigma;br,b'r'} = \psi^{\dagger}_{\sigma rb}\psi_{\bar{\sigma} r'b'}$ can show power-law decay. A list of phases with the corresponding pinned fields and the gapless many-body correlations is given in Table II.

For the phases with three gapped modes, four-particle correlators can be constructed using the bosonization dictionary which do not contain the fields dual to the pinned fields. However, these correlations are of little physical use and we do not give them here explicitly.

V. SPECTRAL FUNCTION AND DENSITY OF STATES

For the system of gold wires on a Ge(001) surface, the density of states (DOS) has been measured experimentally and found to show power-law scaling. As discussed in the previous section, such a power-law scaling will only occur if all modes are gapless, i.e., the system is in the C2S2 phase.

In this section, we will calculate the spectral function $A(q,\omega)$ in the C2S2 phase from which the density of states $\nu(\omega)$ can be obtained by a momentum integration. The spectral function itself may be measurable in a suitable experiment by ARPES. While the DOS gives only information about a certain combination of the Luttinger liquid parameters and thus by itself does not allow a check if the predictions of our model for the extent of the C2S2 phase are consistent with experiment, the spectral function will, in principle, allow one to determine all four Luttinger parameters separately and thus allow a full consistency check.

The spectral function for the interacting fermionic model can be calculated directly using the bosonic Luttinger liquid representation.[51,52] In general, it is defined as $A(k,\omega) = -\frac{1}{\pi}\mathrm{Im}\, G^{\mathrm{ret}}(k,\omega)$, where $G^{\mathrm{ret}}(k,\omega)$ is the retarded Green's function. Equivalently we can write, with $\mathbf{r} = (x,t)$,

$$A(k,\omega) = \frac{1}{2\pi}\sum_{\sigma}\int dx\, dt\, e^{i(\omega t - kx)}\langle\{\psi_{\sigma}(\mathbf{r}),\psi^{\dagger}_{\sigma}(0)\}\rangle. \quad (5.1)$$

After linearization, we are therefore interested in

$$iG^{>}_{\sigma}(\mathbf{r}) = \sum_{br} e^{ir\eta_b k_{Fb}x}\langle\psi_{\sigma br}(\mathbf{r})\psi^{\dagger}_{\sigma br}(0)\rangle, \quad (5.2)$$

and a similar term for $iG^{<}_{\sigma}(\mathbf{r})$ where the two fermionic operators are interchanged. Ignoring the small spin-orbit splitting we can use the bosonic Green's function, Eq. (3.2), and find

$$iG^{>}_{\sigma}(\mathbf{r}) = \frac{1}{2\pi\alpha}\sum_{br} e^{ir\eta_b k_{Fb}x}\prod_{\nu\beta\delta} e^{-\pi\xi^{r}_{\nu\beta\delta}G_{\nu\beta\delta}(\mathbf{r})}, \quad (5.3)$$

where $\delta = \pm$ denotes the chiral component of the field and

$$\xi^{r}_{\nu\beta\delta} = \frac{1}{16}\left[\sqrt{K^{\nu\beta}} - \frac{\delta r}{\sqrt{K^{\nu\beta}}}\right]^2, \quad (5.4)$$

which arises from the rotation between the original $\phi_{\sigma br}$ field and the chiral mode $\phi^{\nu\beta}_{\delta}$. In the space and time representation, this leads to

$$A(\mathbf{r}) \sim \frac{1}{2\pi^2\alpha}\sum_{\sigma br} e^{ir\eta_b k_{Fb}x}\prod_{\nu\beta\delta}\left[\frac{\alpha}{|x - \delta u^{\nu\beta}t|}\right]^{\xi^{r}_{\nu\beta\delta}} \quad (5.5)$$

with

$$A(k,\omega) = \int dx\, dt\, e^{i\omega t - ikx}A(\mathbf{r}). \quad (5.6)$$

This integral cannot be calculated analytically in full but we can obtain the singular contributions[51,52] which occur at $\omega = \pm u^{\nu\beta}|k|$.

Using Eqs. (5.5) and (5.6), the full spectral function can be decomposed into the sum

$$A(k,\omega) = \sum_{rb} A_r(k - r\eta_b k_{Fb},\omega). \quad (5.7)$$

The spectral function has the symmetry $A_+(q,\omega) = A_-(-q,\omega)$, and therefore we focus only on $A_+(q,\omega)$. To calculate these contributions, we first order the four velocities in order of increasing magnitude such that $u^{\nu_1\beta_1} < u^{\nu_2\beta_2} < u^{\nu_3\beta_3} < u^{\nu_4\beta_4}$, where as before $\nu_i = \{c,s\}$ and $\beta_i = \pm$. Then

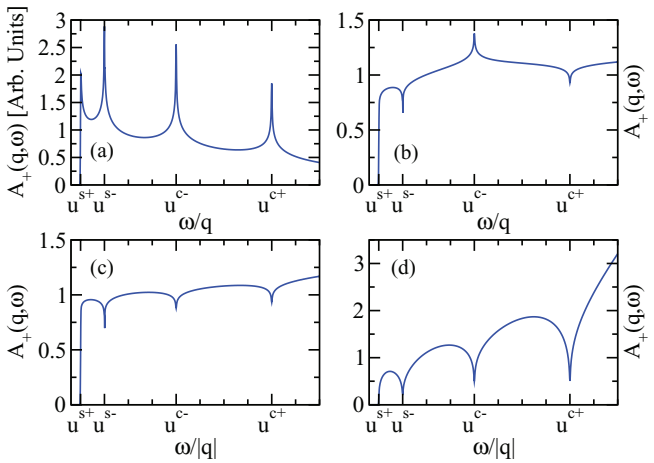

FIG. 6. (Color online) The spectral function, Eq. (5.6). Parts (a) and (c) are plotted for $K^{c+} = K^{c-} = 0.7$, $K^{s+} = 1.3$, and $K^{s-} = 1$. Parts (b) and (d) are plotted for $K^{c+} = 0.3$, $K^{c-} = 0.5$, $K^{s+} = 1.7$, and $K^{s-} = 1.3$. The top row, (a) and (b), is for positive momenta; the bottom row, (c) and (d), is for negative momenta. The spectral function has been convoluted with a Gaussian resolution function of width $\omega/u^{c-}|q| = 0.001$.

we make a relabeling such that $u_i = u^{\nu_i\beta_i}$. Now for positive momenta $q > 0$ we find in the vicinity of $\omega \approx u_1 q$

$$A_r(q,\omega) \sim \Theta(\omega - u_1 q)(\omega - u_1 q)^{[\gamma_1+2\gamma_2+2\gamma_3+2\gamma_4-(r+1)/4]/2}. \tag{5.8}$$

The exponents are given by

$$\gamma_i = \frac{1}{8}\left[K^{\nu_i\beta_i} + \frac{1}{K^{\nu_i\beta_i}} - 2\right]. \tag{5.9}$$

At the remaining singular points, $\omega \approx u_i q$ with $i \in \{2,3,4\}$, the spectral function behaves as

$$A_r(q,\omega) \sim |\omega - u_i q|^{[\gamma_i+2\sum_{j\neq i}\gamma_j-(r+1)/4]/2}. \tag{5.10}$$

The full $A_r(q > 0,\omega)$ is the product over Eqs. (5.8) and (5.10).

For negative momenta, $q < 0$, we find near $\omega \approx u_1|q|$

$$A_r(q,\omega) \sim \Theta(\omega + u_1 q)(\omega + u_1 q)^{[\gamma_1+2\gamma_2+2\gamma_3+2\gamma_4+(r-1)/4]/2}. \tag{5.11}$$

At the remaining singular points, $\omega \approx u_i q$ with $i = \{2,3,4\}$, the spectral function behaves as

$$A_r(q,\omega) \sim |\omega + u_i q|^{[\gamma_i+2\sum_{j\neq i}\gamma_j+(r-1)/4]/2}. \tag{5.12}$$

The spectral function for positive and negative momenta and $r = +$ is plotted in Fig. 6 for two different parameter sets. The slope of the divergences and cusps yields information about the four Luttinger parameters, which would allow a consistency check on our model. The existence of cusps versus divergences is dependent on the values of the Luttinger parameters, as can be seen from a comparison of Figs. 6(a) and 6(b). From Eq. (5.7) one can see that the measured spectral function will consist of four sets of peaks and cusps around the four Fermi points. The two positive Fermi momenta will show the same structure, as will the negative Fermi points.

One of the classic signatures of a Luttinger liquid, taken as an indication of a Luttinger liquid state in the experiment

TABLE III. The exponents for power-law suppression of the DOS near the Fermi energy: $\nu(\omega) \sim \omega^{\gamma}$. Listed are the exponents, γ, for a spinless, a standard single-band, and a two-band Luttinger liquid. Also listed are the cases for SU(2)-symmetric models where $K^{s+} = K^{s-} = K_s = 1$.

Model	General	SU(2)-symmetric
Spinless	$\frac{1}{2}\left[K + \frac{1}{K} - 2\right]$	N.A.
Single- band	$\frac{1}{4}\sum_{\nu}\left[K_\nu + \frac{1}{K_\nu} - 2\right]$	$\frac{1}{4}\left[K_c + \frac{1}{K_c} - 2\right]$
Two-band	$\frac{1}{8}\sum_{\nu\beta}\left[K^{\nu\beta} + \frac{1}{K^{\nu\beta}} - 2\right]$	$\frac{1}{8}\sum_{\beta}\left[K^{c\beta} + \frac{1}{K^{c\beta}} - 2\right]$

of Blumenstein *et al.*[25] on the monatomic gold chains, is the power-law suppression of the DOS near the Fermi energy.[53,54] The experimental result was analyzed with the single-band DOS. Here we now derive the equivalent formula for the appropriate two-band model directly from the spectral function

$$\nu(\omega) \sim \sum_q A(q,\omega) = A(x = 0,\omega)$$
$$\sim \frac{1}{2\pi^2\alpha}\int dt\, e^{i\omega t}\sum_{\sigma br}\prod_{\nu\beta\delta}\left(\frac{\alpha}{\delta u^{\nu\beta} t}\right)^{\xi^r_{\nu\beta\delta}}. \tag{5.13}$$

We are only interested here in the power-law suppression, which can be gained directly by power counting, and gives $\nu(\omega) \sim \omega^{\gamma}$ with the exponent

$$\gamma = \sum_{\nu\beta\delta}\xi^r_{\nu\beta\delta} - 1 = \frac{1}{8}\sum_{\substack{\nu=c,s\\ \beta=\pm}}\left[K^{\nu\beta} + \frac{1}{K^{\nu\beta}} - 2\right]. \tag{5.14}$$

As a comparison, the standard results for this exponent for a spinless as well as for a spinful single-band Luttinger liquid are given in Table III.

Near a boundary the DOS is suppressed with a different exponent. Exactly as in the single-band case, the bulk and boundary exponents are related by a conformal mapping.[2] In the two-band Luttinger liquid, however, the relation between the bulk and the boundary exponent,

$$\gamma^b = \frac{1}{4}\sum_{\substack{\nu=c,s\\ \beta=\pm}}\left[\frac{1}{K^{\nu\beta}} - 1\right], \tag{5.15}$$

is no longer enough to independently check all four Luttinger parameters from DOS measurements alone.

Similarly, the Green's function for finite temperatures can be calculated from the zero-temperature case by a conformal mapping. The standard results for the finite-temperature single-band Luttinger liquid DOS then still apply with a suitably modified exponent.

VI. DISCUSSION AND CONCLUSIONS

Recent experiments on self-organized gold chains on a Ge(001) surface have provided evidence for Luttinger liquid behavior. Other experiments on similar surface systems have shown earlier that spin-orbit coupling effects play an important role for the physics of such systems with both Rashba- and Dresselhaus-type couplings being allowed by

the reduced symmetry. Furthermore, the gold surface band is found to cross the Fermi surface four times giving rise to two separate electron pockets. The combination of spin-orbit coupling, which breaks SU(2) spin rotational symmetry, with the effective two-band structure at low energies makes the gold chains very different from other quasi-one-dimensional systems as, for example, carbon nanotubes or semiconducting nanowires, where Luttinger liquid behavior has also been seen.

In our paper, we considered the low-energy effective theory of a generic two-band model with spin-orbit coupling using bosonization. To simplify the discussion, we made a number of approximations. First, we assumed that the two bands have equal Fermi velocities, $v_{Fb} = v_{F\bar{b}}$. This seems to be approximately the case in the experiments on gold chains. The generalization to the case of unequal velocities is straightforward and is discussed in detail in Appendix B. Having unequal velocities for the two bands is a marginal perturbation when starting from the symmetric band case. It can therefore only affect the phase diagram of the model at second or higher order in the RG flow, which is beyond the scope of this paper. Experimentally, this also means that such effects would only become visible at very low temperatures if the considered system would remain ideally one-dimensional.

Second, we ignored that the spin-orbit coupling leads to an effective mixing of higher transverse modes into the lowest one which can make the velocities of the spin-split band unequal, $v_{Fb\sigma} \neq v_{Fb\bar{\sigma}}$. The better the confinement in the transverse direction is, the smaller is this effect. For the gold chains, the dispersion perpendicular to the chain direction is flat so that assuming a very strong confinement seems to be a good approximation. Allowing for $v_{Fb\sigma} \neq v_{Fb\bar{\sigma}}$ activates additional single spin-flip scattering processes which are otherwise forbidden by symmetry. These scattering processes are, however, always oscillating and therefore cannot modify the zero-temperature phase diagram.

Using these two approximations we bosonized the two-band model with spin-orbit coupling including all scattering terms which are allowed by time-reversal symmetry. A diagonalization of the kinetic part, the density-density type interactions, and the spin-orbit coupling was achieved by three separate rotations followed by a shift in one of the bosonic fields. The remaining backscattering and double spin-flip terms were then treated using a first-order RG. This turns out to be sufficient away from the SU(2) symmetric point where most scattering terms are either relevant or irrelevant. Some of the scattering terms are very slowly oscillating in space due to the spin-orbit induced splitting of the band and can thus be ignored at the lowest temperatures. For this case we did calculate the full phase diagram, which turns out to consist of a Luttinger liquid (C2S2) phase as well as phases where two or three out of the four modes (two spin and two charge) are gapped. At intermediate temperatures $\varepsilon_{\mathrm{SO}}^{b} \ll T \ll \varepsilon_F$, the slowly oscillating scattering terms have to be kept in the RG flow. As a consequence, the spin modes might appear to be thermally activated even if all four modes are gapless at $T = 0$.

For the experiment on gold chains this means that although the reduced spin symmetry and the two bands allow for a large number of scattering processes absent in the SU(2) symmetric single-band case, a Luttinger liquid phase is still present in the $T = 0$ phase diagram. This was by no means *a priori* clear and shows that such a system could indeed be a useful test bed for Luttinger liquid physics. Furthermore, our theoretical study makes a clear prediction about the behavior of the density of states and, more importantly, the full spectral function in the C2S2 phase. While the derived formula for the density of states shows that the exponent of the power-law scaling in frequency does not depend on a single Luttinger parameter as assumed in experiment but rather on the four Luttinger parameters $K^{c\pm}$, $K^{s\pm}$, this by itself does not allow one to verify if the predictions of the Luttinger model are consistent with experiment. Here, additional measurements would be desirable. First, the extent of the Luttinger liquid regime in the phase diagram is restricted, limiting the possible values for the Luttinger parameters. From the limits on the Luttinger parameters $K^{s\pm}$ we can, in particular, infer the decay of the spin-spin correlations, which potentially can be tested in experiment by spin-resolved STS. Probably even more promising is the measurement of the full spectral function by ARPES, which, in principle, allows for the determination of all four Luttinger parameters separately and therefore for a full consistency check with the appropriate Luttinger model treated in this paper.

ACKNOWLEDGMENTS

The authors thank I. Affleck and A. Schulz for valuable discussions. We also acknowledge support by the DFG via the SFB/TR 49 and by the graduate school of excellence MAINZ.

APPENDIX A: BOSONIZATION DICTIONARY

Two useful formulas for bosonization are the vertex operator

$$\psi_{\sigma br}(x) \sim \frac{1}{\sqrt{2\pi\alpha}} e^{ir\sqrt{2\pi}\phi_{\sigma br}(x)} \tag{A1}$$

and the densities

$$\rho_{\sigma rb}(x) = \psi^{\dagger}_{\sigma br}(x)\psi_{\sigma br}(x) = -\frac{1}{\sqrt{2\pi}}\partial_x \phi_{\sigma br}(x). \tag{A2}$$

The relation between these bosonic fields and the bosonic fields describing the diagonal normal modes is

$$\begin{aligned}\phi_{\sigma br} = \frac{1}{\sqrt{8}}[&\phi^{c+} + (-1)^b\phi^{c-} + \sigma[\phi^{s+} + (-1)^b\phi^{s-}] \\ &- r\{\theta^{c+} + (-1)^b\theta^{c-} + \sigma[\theta^{s+} + (-1)^b\theta^{s-}]\}].\end{aligned} \tag{A3}$$

The chiral fields ($\delta = \pm$) are in turn determined by

$$\phi_{\delta}^{\nu\beta} = \frac{1}{\sqrt{2}}\left(\frac{\phi^{\nu\beta}}{\sqrt{K^{\nu\beta}}} - \delta\sqrt{K^{\nu\beta}}\theta^{\nu\beta}\right). \tag{A4}$$

APPENDIX B: DIAGONALIZATION FOR ASYMMETRIC BANDS

Here we describe the full diagonalization procedure which holds for nonsymmetric bands. Below the spin and charge indices have been suppressed, but the following applies to

both the spin and charge sector (separately). If we have

$$\begin{pmatrix}\phi_1(x)\\ \phi_2(x)\end{pmatrix}=\begin{pmatrix}T^{\phi}_{11} & T^{\phi}_{12}\\ T^{\phi}_{21} & T^{\phi}_{22}\end{pmatrix}\begin{pmatrix}\tilde{\phi}_1(x)\\ \tilde{\phi}_2(x)\end{pmatrix},$$
$$\begin{pmatrix}\theta_1(x)\\ \theta_2(x)\end{pmatrix}=\begin{pmatrix}T^{\theta}_{11} & T^{\theta}_{12}\\ T^{\theta}_{21} & T^{\theta}_{22}\end{pmatrix}\begin{pmatrix}\tilde{\theta}_1(x)\\ \tilde{\theta}_2(x)\end{pmatrix}, \tag{B1}$$

then we require $[\mathbf{T}^{\phi}]^T=[\mathbf{T}^{\theta}]^{-1}$ for the canonical commutation relations to remain fulfilled for the transformed fields. There are several ways to do this. The important point to note is that it cannot be done with an orthogonal transformation which merely rotates the matrices.

We define $\mathbf{T}^{\phi}=\mathbf{P}\Lambda\mathbf{Q}\tilde{\Lambda}$ and $\mathbf{T}^{\theta}=\mathbf{P}\Lambda^{-1}\mathbf{Q}\tilde{\Lambda}^{-1}$, which automatically ensures that the commutation relations are held. $\mathbf{P}$ and $\mathbf{Q}$ are usual rotations (i.e., orthogonal matrices), and Λ and $\tilde{\Lambda}$ are diagonal matrices which rescale the fields. The idea is that first we rotate and rescale such that $\Lambda\mathbf{P}^T\mathbf{M}'_{\phi}\mathbf{P}\Lambda=\mathcal{I}$, the identity matrix. We then define $\mathbf{N}_{\theta}=\Lambda\mathbf{P}^T\mathbf{M}'_{\theta}\mathbf{P}\Lambda$, which is now a known symmetric matrix. This we diagonalize with $\mathbf{Q}$, which will of course leave the identity matrix unaffected. Finally, we have a rescaling $\tilde{\Lambda}$ so that $\tilde{\theta}$ and $\tilde{\phi}$ have the same eigenvalues.

The two rescalings are $\Lambda=\mathrm{diag}(\lambda_1^{-\frac{1}{2}},\lambda_2^{-\frac{1}{2}})$ and $\tilde{\Lambda}=\mathrm{diag}(\tilde{\lambda}_1^{-\frac{1}{2}},\tilde{\lambda}_2^{-\frac{1}{2}})$ with

$$\lambda_{1,2}=\frac{v_1}{2K_1}+\frac{v_2}{2K_2}\pm\sqrt{v_B^2+\left(\frac{v_1}{2K_1}-\frac{v_2}{2K_2}\right)^2} \tag{B2}$$

and

$$\frac{1}{\tilde{\lambda}_{1,2}}=\sqrt{\frac{N^{\theta}_{11}}{2}+\frac{N^{\theta}_{22}}{2}\pm\sqrt{\left[N^{\theta}_{12}\right]^2+\left(\frac{N^{\theta}_{11}}{2}-\frac{N^{\theta}_{22}}{2}\right)^2}}. \tag{B3}$$

Therefore, in the end $\mathbf{M}_{\phi}=\mathbf{M}_{\theta}=\mathrm{diag}[u_1,u_2]$ with

$$(u_{1,2})^2=\frac{N^{\theta}_{11}}{2}+\frac{N^{\theta}_{22}}{2}\pm\sqrt{\left[N^{\theta}_{12}\right]^2+\left(\frac{N^{\theta}_{11}}{2}-\frac{N^{\theta}_{22}}{2}\right)^2}. \tag{B4}$$

The Hamiltonian becomes

$$H_q=\sum_{\substack{\nu=c,s\\ \beta=1,2}}\frac{u_{\nu\beta}}{2}\int dx[[\partial_x\tilde{\phi}^{\nu\beta}(x)]^2+[\tilde{\Pi}^{\nu\beta}(x)]^2]. \tag{B5}$$

Note that contrary to the basis used in the main text, we have here rescaled the Luttinger parameters out of the Hamiltonian, equivalent to $\phi^{\nu\beta}\to\tilde{\phi}^{\nu\beta}\sqrt{K^{\nu\beta}}$ and $\theta^{\nu\beta}\to\tilde{\theta}^{\nu\beta}/\sqrt{K^{\nu\beta}}$.

The generalization of the SU(2) symmetry condition on the Luttinger parameters, see Sec. III, for asymmetric bands leads to the condition $\mathbf{T}^{\phi}_s=\mathbf{T}^{\theta}_s$, or equivalently $\Lambda_s\mathbf{Q}_s\tilde{\Lambda}_s=\Lambda_s^{-1}\mathbf{Q}_s\tilde{\Lambda}_s^{-1}$. This in turn tells us that $\lambda_{s1}=\lambda_{s2}=\tilde{\lambda}_{s1}^{-1}=\tilde{\lambda}_{s2}^{-1}$ and from this the conditions $v_{sA}=v_{sB}=0$, $K_{s1}=K_{s2}=1$, and $v_{s1}=v_{s2}$ follow directly. That is, for an SU(2) symmetric system the spin part of the Hamiltonian is already diagonal in the band indices. It is therefore of course also diagonal in the $\beta=\pm$ basis.

APPENDIX C: EXPRESSIONS FOR VELOCITIES AND LUTTINGER PARAMETERS

In this appendix we give low-order expansions for the velocities in terms of the bare interaction parameters and Fermi velocities. Note that as before all kinematically indistinct processes are assumed to be already appropriately rescaled. The velocities and interband coupling terms are, for the spin sector,

$$\begin{aligned}v_{sA}&=\frac{2\bar{g}_{4\parallel}-\bar{g}_{4\perp}-2\bar{g}_{2\parallel}+\bar{g}_{2\perp}}{16\pi},\\ v_{sB}&=\frac{2\bar{g}_{4\parallel}+\bar{g}_{4\perp}-2\bar{g}_{2\parallel}-\bar{g}_{2\perp}}{16\pi},\\ v_{sb}^2&=\left(v_{Fb}-\frac{2g_{2b\parallel}-g_{2b\perp}-4g_{4\parallel b}+2g_{4\perp b}}{8\pi}\right)\\ &\quad\times\left(v_{Fb}-\frac{2g_{2b\parallel}+g_{2b\perp}-4g_{4\parallel b}-2g_{4\perp b}}{8\pi}\right)\end{aligned} \tag{C1}$$

with band index $b=\{1,2\}$. In the charge sector, we have

$$\begin{aligned}v_{cA}&=\frac{2\bar{g}_{4\parallel}-\bar{g}_{4\perp}+2\bar{g}_{2\parallel}-\bar{g}_{2\perp}}{16\pi},\\ v_{cB}&=\frac{2\bar{g}_{4\parallel}+\bar{g}_{4\perp}+2\bar{g}_{2\parallel}+\bar{g}_{2\perp}}{16\pi},\\ v_{cb}^2&=\left(v_{Fb}+\frac{2g_{2b\parallel}-g_{2b\perp}+4g_{4\parallel b}-2g_{4\perp b}}{8\pi}\right)\\ &\quad\times\left(v_{Fb}+\frac{2g_{2b\parallel}+g_{2b\perp}+4g_{4\parallel b}+2g_{4\perp b}}{8\pi}\right).\end{aligned} \tag{C2}$$

The Luttinger parameters are

$$\begin{aligned}K_{sb}^2&=\left(v_{Fb}-\frac{2g_{2b\parallel}-g_{2b\perp}-4g_{4\parallel b}+2g_{4\perp b}}{8\pi}\right)\\ &\quad\times\left(v_{Fb}-\frac{2g_{2b\parallel}+g_{2b\perp}-4g_{4\parallel b}-2g_{4\perp b}}{8\pi}\right)^{-1}\end{aligned} \tag{C3}$$

and for the charge sector

$$\begin{aligned}K_{cb}^2&=\left(v_{Fb}+\frac{2g_{2b\parallel}-g_{2b\perp}+4g_{4\parallel b}-2g_{4\perp b}}{8\pi}\right)\\ &\quad\times\left(v_{Fb}+\frac{2g_{2b\parallel}+g_{2b\perp}+4g_{4\parallel b}+2g_{4\perp b}}{8\pi}\right)^{-1}.\end{aligned} \tag{C4}$$

The multitude of g parameters will depend on the specific microscopic model under consideration.

For the symmetric band model which we consider in the main text, we find, with $v_{\nu b}=v_{\nu}$ and $K_{\nu b}=K_{\nu}$,

$$\begin{aligned}(u^{\nu\pm})^2&=(v_{\nu}\pm v_{\nu B}K_{\nu})(v_{\nu}\pm v_{\nu A}/K_{\nu}),\\ \frac{1}{(K^{\nu\pm})^2}&=\frac{1}{K_{\nu}^2}\frac{v_{\nu}\pm v_{\nu B}K_{\nu}}{v_{\nu}\pm v_{\nu A}/K_{\nu}}\end{aligned} \tag{C5}$$

for the velocities and Luttinger parameters of the normal modes.

APPENDIX D: INTERACTIONS WITH FINITE MOMENTUM TRANSFER

At special fillings where the total transferred momentum in a scattering process becomes commensurate with the lattice, additional interactions to those considered in Sec. II

can become important. For completeness we list them here. For $2(k_{F1}+k_{F2})=2\pi$ we have the following additional processes, which we have neglected. First,

$$\begin{aligned}\bar{H}_1 &= \sum_{\sigma,\sigma',b,r}\int dx\,\frac{\bar{g}_1}{2}\psi^\dagger_{\sigma'\bar{b}r}\psi_{\sigma'\bar{b}\bar{r}}\psi^\dagger_{\sigma b\bar{r}}\psi_{\sigma br},\\ \bar{H}'_{2\perp} &= \sum_{\sigma,b,r}\int dx\,\frac{\bar{g}'_{2\perp}}{2}\psi^\dagger_{\bar{\sigma}b\bar{r}}\psi_{\bar{\sigma}\bar{b}\bar{r}}\psi^\dagger_{\sigma\bar{b}r}\psi_{\sigma br},\\ H'_{4\perp} &= \sum_{\sigma,\sigma',b,r}\int dx\,\frac{g'_{4\perp}}{2}\psi^\dagger_{\sigma'\bar{b}r}\psi_{\sigma'br}\psi^\dagger_{\sigma\bar{b}r}\psi_{\sigma br}.\end{aligned}\tag{D1}$$

Bosonized they are, first,

$$\begin{aligned}\bar{H}_{1\parallel} &= \frac{\bar{g}_{1\parallel}}{(\pi\alpha)^2}\int dx\,\cos[\sqrt{4\pi}\phi^{s-}]\cos[\sqrt{4\pi}\phi^{c-}],\\ \bar{H}_{1\perp} &= \frac{\bar{g}'_{2\perp}}{(\pi\alpha)^2}\int dx\,\cos[\sqrt{4\pi}\phi^{s+}]\cos[\sqrt{4\pi}\phi^{c-}],\\ \bar{H}'_{2\perp} &= \frac{\bar{g}'_{2\perp}}{(\pi\alpha)^2}\int dx\,\cos[\sqrt{4\pi}\theta^{s-}]\cos[\sqrt{4\pi}\phi^{c-}].\end{aligned}\tag{D2}$$

Finally,

$$\begin{aligned}H'_{4\parallel} &= \frac{g'_{4\parallel}}{(\pi\alpha)^2}\int dx\\ &\quad\times\Big\{\prod_\nu \cos[\sqrt{4\pi}\phi^{\nu-}]\cos[\sqrt{4\pi}\theta^{s-}]\cos[\sqrt{4\pi}\theta^{c-}]\\ &\quad+\prod_\nu \sin[\sqrt{4\pi}\phi^{\nu-}]\sin[\sqrt{4\pi}\theta^{s-}]\sin[\sqrt{4\pi}\theta^{c-}]\Big\},\\ H'_{4\perp} &= \frac{g'_{4\perp}}{(\pi\alpha)^2}\int dx\,\cos[\sqrt{4\pi}\phi^{c-}]\cos[\sqrt{4\pi}\theta^{c-}].\end{aligned}\tag{D3}$$

There is also a particular umklapp process for which the oscillations can become commensurate with the lattice. This is a $3k_{F2}-k_{F1}$ momentum transfer process:

$$H_U = g_U\sum_{\sigma,\sigma',b,r}\int dx\,e^{-ir(3k_{F2}-k_{F1})x}\psi^\dagger_{\sigma'\bar{b}\bar{r}}\psi_{\sigma'br}\psi^\dagger_{\sigma 2\bar{r}}\psi_{\sigma 2r}.\tag{D4}$$

In the bosonic form this becomes

$$\begin{aligned}H_U &= \frac{g_U}{(\pi\alpha)^2}\sum_\sigma\int dx\,\cos[\sqrt{\pi}(\theta^{c-}-\sigma\theta^{s-})]\\ &\quad\times\cos[(3k_{F2}-k_{F1})x-\sqrt{\pi}(\sqrt{4}\phi^{c+}-\phi^{c-}-\sigma\phi^{s-})].\end{aligned}\tag{D5}$$

In particular, though not solely, one can see that this umklapp scattering term will become important for the highly symmetric scenario $k_{F2}=3k_{F1}=3\pi/4$ as then $3k_{F2}-k_{F1}=2\pi$. In this case all of these momentum transfer processes listed in this appendix will be present.

The scaling dimensions of these interactions necessary for the first-order RG equations are, in the band symmetric model,

$$\begin{aligned}\bar{\gamma}_{1\parallel} &= K^{s-}+K^{c-},\quad \bar{\gamma}_{1\perp}=K^{s+}+K^{c+},\\ \bar{\gamma}'_{2\perp} &= K^{c-}+\frac{1}{K^{s-}},\quad \gamma'_{4\perp}=K^{c-}+\frac{1}{K^{c-}},\\ \gamma'_{4\parallel} &= K^{s-}+K^{c-}+\frac{1}{K^{s-}}+\frac{1}{K^{c-}},\\ \gamma_U &= K^{c+}+\frac{1}{4}\left[K^{s-}+K^{c-}+\frac{1}{K^{s-}}+\frac{1}{K^{c-}}\right].\end{aligned}\tag{D6}$$

$g'_{4\parallel}$ is irrelevant and $g'_{4\perp}$ is at best marginal. In the general non-SU(2)-symmetric case we consider, the rest would have to be taken into account. In principle, all of these processes can also show up in the double and single spin-flip versions as well. An exhaustive list of all these possibilities and their influence on the phase diagram is beyond the scope of this paper.

*sedlmayr@physik.uni-kl.de

[1] F. D. M. Haldane, J. Phys. C **14**, 2585 (1981).
[2] T. Giamarchi, *Quantum Physics in One Dimension* (Clarendon, Oxford, 2004).
[3] N. Motoyama, H. Eisaki, and S. Uchida, Phys. Rev. Lett. **76**, 3212 (1996).
[4] M. Hase, I. Terasaki, and K. Uchinokura, Phys. Rev. Lett. **70**, 3651 (1993).
[5] D. C. Dender, P. R. Hammar, D. H. Reich, C. Broholm, and G. Aeppli, Phys. Rev. Lett. **79**, 1750 (1997).
[6] S. Eggert and I. Affleck, Phys. Rev. B **46**, 10866 (1992).
[7] S. Eggert, I. Affleck, and M. Takahashi, Phys. Rev. Lett. **73**, 332 (1994).
[8] M. Oshikawa and I. Affleck, Phys. Rev. Lett. **79**, 2883 (1997).
[9] J. Sirker, N. Laflorencie, S. Fujimoto, S. Eggert, and I. Affleck, Phys. Rev. Lett. **98**, 137205 (2007).
[10] J. Sirker, S. Fujimoto, N. Laflorencie, and S. Eggert, and I. Affleck, J. Stat. Mech. (2008) P02015.
[11] J. Sirker, R. G. Pereira, and I. Affleck, Phys. Rev. Lett. **103**, 216602 (2009).
[12] J. Sirker, R. G. Pereira, and I. Affleck, Phys. Rev. B **83**, 035115 (2011).
[13] R. G. Pereira, J. Sirker, J.-S. Caux, R. Hagemans, J. M. Maillet, S. R. White, and I. Affleck, Phys. Rev. Lett. **96**, 257202 (2006).
[14] R. G. Pereira, J. Sirker, J.-S. Caux, R Hagemans, J. M. Maillet, S. R. White, and I. Affleck, J. Stat. Mech. (2007) P08022.
[15] O. M. Auslaender, H. Steinberg, A. Yacoby, Y. Tserkovnyak, B. I. Halperin, K. W. Baldwin, L. N. Pfeiffer, and K. W. West, Science **308**, 88 (2005).
[16] Z. Yao, H. W. C. Postma, L. Balents, and C. Dekker, Nature (London) **402**, 273 (1999).
[17] M. Bockrath, D. H. Cobden, J. Lu, A. G. Rinzler, R. E. Smalley, L. Balents, and P. L. McEuen, Nature (London) **397**, 598 (1999).
[18] Y. Jompol, C. J. B. Ford, J. P. Griffiths, I. Farrer, G. A. C. Jones, D. Anderson, D. A. Ritchie, T. W. Silk, and A. J. Schofield, Science **325**, 597 (2009).
[19] V. V. Deshpande, M. Bockrath, L. I. Glazman, and A. Yacoby, Nature (London) **464**, 209 (2010).
[20] P. Segovia, D. Purdie, M. Hengsberger, and Y. Baer, Nature (London) **402**, 504 (1999).

[21]R. Losio, K. N. Altmann, A. Kirakosian, J.-L. Lin, D. Y. Petrovykh, and F. J. Himpsel, Phys. Rev. Lett. **86**, 4632 (2001).
[22]J. R. Ahn, H. W. Yeom, H. S. Yoon, and I.-W. Lyo, Phys. Rev. Lett. **91**, 196403 (2003).
[23]D. Sánchez-Portal, S. Riikonen, and R. M. Martin, Phys. Rev. Lett. **93**, 146803 (2004).
[24]I. Barke, F. Zheng, T. K. Rügheimer, and F. J. Himpsel, Phys. Rev. Lett. **97**, 226405 (2006).
[25]C. Blumenstein, J. Schäffer, S. Mietke, S. Meyer, A. Dollinger, M. Lochner, X. Cui, L. Patthey, R. Matzdorf, and R. Claessen, Nat. Phys. **7**, 776 (2011).
[26]J. Schäfer, C. Blumenstein, S. Meyer, M. Wisniewski, and R. Claessen, Phys. Rev. Lett. **101**, 236802 (2008).
[27]S. Meyer, J. Schäfer, C. Blumenstein, P. Höpfner, A. Bostwick, J. L. McChesney, E. Rotenberg, and R. Claessen, Phys. Rev. B **83**, 121411 (2011).
[28]R. Winkler, *Spin-Orbit Coupling Effects in Two-Dimensional Electron and Hole Systems* (Springer, Berlin, 2003).
[29]P. Höpfner, J. Schäfer, A. Fleszar, J. H. Dil, B. Slomski, F. Meier, C. Loho, C. Blumenstein, L. Patthey, W. Hanke *et al*., Phys. Rev. Lett. **108**, 186801 (2012).
[30]A. Schulz, A. De Martino, and R. Egger, Phys. Rev. B **82**, 033407 (2010).
[31]S. Gangadharaiah, J. Sun, and O. A. Starykh, Phys. Rev. B **78**, 054436 (2008).
[32]A. Schulz, A. De Martino, P. Ingenhoven, and R. Egger, Phys. Rev. B **79**, 205432 (2009).
[33]C. M. Varma and A. Zawadowski, Phys. Rev. B **32**, 7399 (1985).
[34]K. Penc and J. Sólyom, Phys. Rev. B **41**, 704 (1990).
[35]A. M. Finkel'stein and A. I. Larkin, Phys. Rev. B **47**, 10461 (1993).
[36]M. Fabrizio, Phys. Rev. B **48**, 15838 (1993).
[37]D. V. Khveshchenko and T. M. Rice, Phys. Rev. B **50**, 252 (1994).
[38]L. Balents and M. P. A. Fisher, Phys. Rev. B **53**, 12133 (1996).
[39]M. Tsuchiizu and A. Furusaki, Phys. Rev. B **66**, 245106 (2002).
[40]M. Tsuchiizu and Y. Suzumura, Phys. Rev. B **72**, 075121 (2005).
[41]P. Chudzinski, M. Gabay, and T. Giamarchi, Phys. Rev. B **78**, 075124 (2008).
[42]R. Noack, S. White, and D. Scalapino, Physica C **270**, 281 (1996).
[43]D. V. Khveshchenko, Phys. Rev. B **50**, 380 (1994).
[44]N. Sedlmayr, S. Eggert, and J. Sirker, Phys. Rev. B **84**, 024424 (2011).
[45]N. Sedlmayr, J. Ohst, I. Affleck, J. Sirker, and S. Eggert, Phys. Rev. B **86**, 121302 (2012).
[46]N. Sedlmayr, P. Adam, and J. Sirker, Phys. Rev. B **87**, 035439 (2013).
[47]T. Giamarchi and H. Schulz, J. Phys. France **49**, 819 (1988).
[48]M.-S. Chang and I. Affleck, Phys. Rev. B **76**, 054521 (2007).
[49]I. Garate and I. Affleck, Phys. Rev. B **81**, 144419 (2010).
[50]G. Jüttner, A. Klümper, and J. Suzuki, Nucl. Phys. B **522**, 471 (1998).
[51]V. Meden and K. Schonhammer, Phys. Rev. B **46**, 15753 (1992).
[52]J. Voit, Rep. Prog. Phys. **58**, 977 (1995).
[53]B. Braunecker, C. Bena, and P. Simon, Phys. Rev. B **85**, 035136 (2012).
[54]D. Schuricht, S. Andergassen, and V. Meden, J. Phys.: Condens. Matter **25**, 014003 (2013).